Journal of Visualization, Vol. 9, No. 2 (2006)219-226

Characterization of a Diffuser Flow by Time-Resolved PIV

Vétel, J.*, Farinas, M. -I.*, Garon, A.* and Pelletier, D.*

* Mechanical Engineering Department, École Polytechnique de Montréal, P.O. Box 6079 Station Centre ville, Montréal (Québec), CANADA, H3C 3A7. E-mail: Marie-Isabelle.Farinas@polymtl.ca

Received 28 October 2005
Revised 26 January 2006

Abstract : Computational fluid dynamics is extensively used in the design methodology of medical devices. However, for such applications, the predictive capabilities of CFD codes are highly dependent upon geometry, which most of the time is extremely complex, and flow conditions. The study concerns a ventricular assist device (VAD) where the exit flow, generated through a diffuser, is of particular importance for blood damage predictions. The difficulty to predict the flow lies in the fact that the Reynolds number range includes the transition Reynolds number of the separated diffuser flow as well as the critical Reynolds number of pipe flows. In order to choose the appropriate CFD methodology in terms of flow hypothesis and turbulence model, an experimental setup of the diffuser was built to run PIV velocity measurements and to analyze the flow pattern with the influence of Reynolds number. The flow is described with mean and variance values of the in-plane velocity components and time-resolved results are used to visualize the development of unsteady phenomena introduced in the diffuser separated region. An optimal filter is also used to remove noise in measured velocity vector fields.

Keywords : Diffuser flow, Axisymmetric constriction, Time-resolved PIV, Wiener filter.

1. Introduction

Arterial and heart diseases are commonly related to flow mechanisms, motivating numerous laboratory studies in biomechanics and bioengineering mechanics. Fluid dynamics within arteries has first been investigated through experimental idealized situations as for example the modeling of stenosed arteries by smooth axisymmetric constrictions. Nowadays, computational fluid dynamics is extensively used in arterial flows involving complex geometries or fluid-structure interaction. Indeed exhaustive experimental results for these cases are difficult to find, notwithstanding the fact that they represent almost the only way to design medical devices.

Under standard physiological flow conditions, arterial flows are usually considered to be laminar. However, in the presence of heart valves, catheters or ventricular assist devices, the flow is unsteady and usually presents separations so that turbulence can appear as a non-desirable phenomenon. For example, thrombosis, which is closely related to shear-stress, represents an extremely important phenomenon due to its close link to cardiovascular system diseases. Therefore, instability and transition to turbulence is an important factor to take into account in artery flows under non-natural flow conditions.

The study presented in this paper deals with a ventricular assist device. The blood pump comprises an inlet stator, a rotor, an outflow stator and a diffuser. The fact that such devices work with a steady mean flow instead of the natural pulsatile blood flow is susceptible to induce non-natural dynamic phenomena in arteries. The aim of the study is then to investigate experimentally

the pipe flow downstream of the diffuser for the characterization of the unsteady flow development. As a first step, the flow rotation generated from the action of the rotor is neglected. Previous works on diffusers deal mainly with geometries with an upstream corner, formed by the inlet channel wall and the deflected wall, and a downstream corner, formed by the deflected wall and the outlet channel wall. Usually the configuration is planar and the diffuser is symmetric or asymmetric; the focus of these studies is separation and reattachment points (a review on separating flows can be found in Simpson, 1989). However, the diffuser used here presents a smooth axisymmetric constriction, and therefore no direct comparisons can be made.

Basically, the smooth axisymmetric constriction is similar, for the downstream flow condition, to the idealized representation of a stenosed artery with a 75 % restriction area (Berger and Jou, 2000). In the past, hot wire measurements (Ahmed and Giddens, 1983; Ahmed, 1998) were used to describe turbulence characteristics. Research on separated flow physics has been hindered by the fact that conventional hot-wire measurement technique is direction insensitive. With increasing use of LDA technique more data for separated flows are becoming available which are suitable for validation purposes, but inherently fail to depict the instantaneous flow pattern. Particle image velocimetry measurements are now a common feature in biomechanics studies where spatial description of the flow structures is of primary importance. The objective is to exploit the ability of time-resolved PIV to describe unsteady mechanisms leading to turbulence transition in the diffuser. The flow is described in terms of turbulent statistics and a particular attention is reported on signal processing technique used in the frequency domain to remove noise and hence to improve results.

2. Experimental Setup and Measuring Techniques

2.1 Test Circuit

The circuit consists of a recirculating test rig with an optically clear pipe downstream of the diffuser. The driving system is provided by a medical centrifugal pump (BPX80, Medtronic Inc.) with an electromagnetic flow meter (BIO Probe TX40, Medtronic Inc.) at the exit. A straight tube is placed upstream the diffuser to insure a uniform flow at the entrance, and a discharge tank completes the test bench. Figure 1 presents a schematic cut of the diffuser whose geometry is represented by an axisymmetric smooth nozzle. The internal diameter D of the pipe at the downstream end of the diffuser is 15.8 mm while the maximum reduction in radius reaches 50 %, which corresponds to a 75 % reduction in area. Only the straight pipe at the diffuser outlet is transparent.

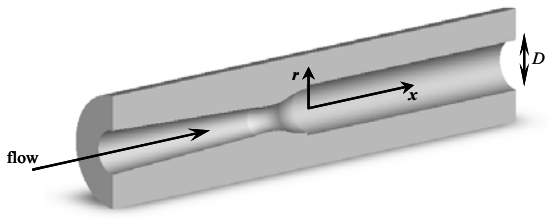

Fig. 1. Sketch of the diffuser.

The model is made with optically clear acrylic. A water-glycerin mixture (40 % glycerin in weight) is used both as a blood analog and as a partial refractive index matching fluid. The density ρ of the mixture is 1.1 kg/l while the kinematic viscosity υ is 3.327 10^{-6} m²/s. The x axis coincides with the pipe axis and originates at the diffuser outlet. The velocities in the axial and radial directions are noted by u and v, respectively. For a given mass flow rate, the sectional average velocity $\overline{u}_m$ is computed based on the diameter D and the Reynolds number is defined by $Re = \overline{u}_m D / \upsilon$.

2.2 PIV Measurements

The working fluid is seeded with fluorescent tracer particles (Rhodamin B-particles) with a mean

diameter around 10 μm, which allows the use of an optical band-pass filter in front of the lens to remove direct reflections of the laser light. The flow is illuminated with a Dantec Dynamics time-resolved laser which is a cw-diode pumped, Q-switched and frequency doubled Nd:YAG laser, suitable for generation of short pulses at high repetition rates. A high speed CMOS camera (Dantec Dynamics NanoSense TR camera) is synchronized with the laser pulses. The camera is able to record full resolution images (1280 × 1024 pixels) at frame rates up to 300 Hz in double-frame mode. Higher frame rates are available with partial readout of the image sensor camera, depending on the selected image area size. Usually, in the experiments reported here, resolution is 1280 × 320 pixels. This field of view was chosen in order to obtain a large field area to visualize spatial development of unsteady flow. The number of total frames within one recording period is limited as a result from the maximum of digital memory available in the camera control unit. The treatment used for the cross-correlation is an adaptive multi-pass correlation in the 32 × 16 pixel interrogation area with an overlap of 50 %. The vectors with a signal/noise ratio below 1.2 are filtered by the median filter.

2.3 Signal Processing

Data acquisition for statistical and spectral analysis was performed at a sampling frequency of 500 Hz. Due to limited camera memory, typically 6 independent sets of approximately 1500 vector fields were acquired. Estimation of the first and second moments results from an average over the entire data (more than 9000 samples). An example of statistical results is presented in Fig. 2 using axial and radial velocities measured at a location where large fluctuations are observed. k is the number of temporal velocity data used in the averaging process. Mean velocities $\overline{u}$ and $\overline{v}$, turbulence velocity q and shear-stress $\overline{u'v'}$ reach a satisfactory statistical convergence when computed with the entire available data sets.

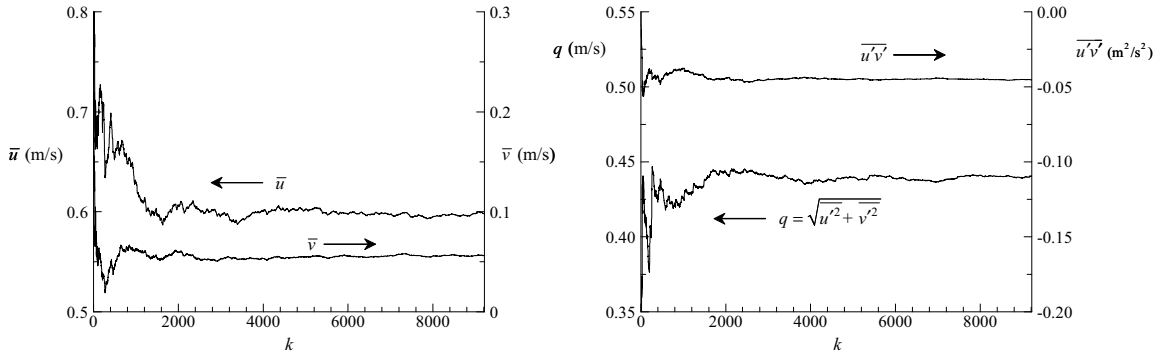

Fig. 2. Statistical convergence of mean velocities and mean fluctuations.

Figure 3 presents an example of an axial velocity fluctuation time signal $c\,(t\,)$ in a non-turbulent region of the flow and the associated power spectrum calculated with an average of 138 blocks of 128 data points. For highest frequencies (f > 200 Hz), an almost constant energy signal is found and can be assimilated to white noise. The origin of this noise is thought to come from the experimental and flow conditions. First, the thickness of laser light sheet is approximately 1-2 mm and this value is high compared to the 15.8 mm diameter diffuser. Hence the image quality was compensated with a short laser pulse to minimize the particle displacement in the direction normal to the light sheet. Second, in investigating the case of small Reynolds numbers, unsteady phenomena develop in a large area so that a large field of view was chosen for PIV measurements. Another reason for presence of noise is that the flow is characterized by a turbulent behavior for relatively small Reynolds numbers. Therefore, velocity gradients induced by flow fluctuations limit the use of large interrogation windows despite the small mean velocity levels.

In the example of Fig. 3, the noise represents an important part of the fluctuating signal since flow perturbations are weak in this region and the objective is to remove it. In an attempt to correct the signal, Son and Kihm (2001) used a temporal post-processing algorithm similar to spatial post-processing used in PIV velocity vector validation scheme by comparisons of neighboring

vectors. However, their objective was to remove erroneous vectors resulting from presence of bubbles in the flow. A different approach, based on filtering, is used here since the objective is to remove noise inherently induced by the measurement process. If the measured signal $c(t)$ contains an additional component of noise $n(t)$, then $c(t) = u(t) + n(t)$ where $u(t)$ is the uncorrupted signal we want to analyze. The objective is to find the optimal filter, $\phi(f)$ in the spectral domain, which, when applied to the measured signal $c(t)$ or $C(f)$ produces a signal $\tilde{u}(t)$ or $\tilde{U}(f)$ that is as close as possible to the uncorrupted signal $u(t)$ or $U(f)$. The true signal is then estimated by $\tilde{U}(f) = C(f).\phi(f)$, and in the least-square sense, minimization of the difference between corrupted and uncorrupted signals leads to:

$$\phi(f) = \frac{|U(f)|^2}{|U(f)|^2 + |N(f)|^2}$$

which is called the Wiener filter. To determine it, it is possible to use the power spectral density:

$$|U(f)|^2 + |N(f)|^2 \approx |C(f)|^2$$

The power spectrum computed with blocks of 16 data points (more than 1000 averages) and using the zero-padding technique for additional interpolated points is plotted in Fig. 3. It can be seen that the true signal is added to a smoothly varying noise. A curve is deduced from the noise and extrapolated back into the signal region as a kind of noise model. The difference between this curve and the signal is used as model of signal power, and quotient of this quantity to signal power plus noise gives the function $\phi(f)$. When applied to measured signal $c(t)$, the filtered signal obtained becomes a smooth function of time and main part of noise has been removed.

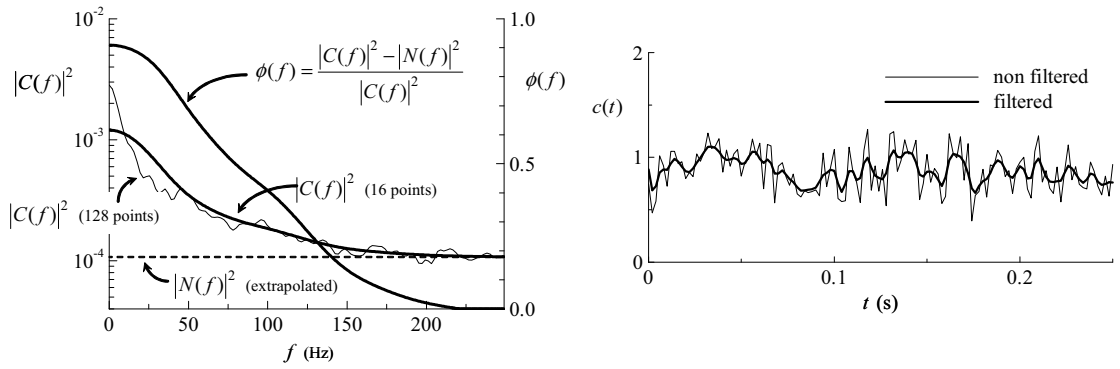

Fig. 3. Procedure used for determination of filter function.

An example of data improvement using the Wiener filter is illustrated in Fig. 4 with an instantaneous velocity vector map obtained for $Re = 2000$. The reference velocity $\bar{u}_m$ was subtracted from the axial velocity to emphasize the vortical structure of the flow. The raw velocity data points out the vortical flow behavior as for example the presence of two vortices whose centers are approximately located at $r/D = 0.3$, $x/D = 0.2$ and $x/D = 0.8$. The turbulence is represented as well by vectors involving a large range of amplitudes and orientations. The associated streamlines are also shown from obviously a qualitative point of view since they are computed with two components of the velocity vector which is three-dimensional by nature in turbulent flows. However the two vortices are clearly shown even if some streamlines show irregularity. Comparatively, when measured velocities are treated again with the Wiener filter, the velocity vector map is smoother than the raw vectors. While the filtering approach, performed in the frequency domain, is applied to each velocity time signals and is independent of adjacent points, quite good results are obtained regarding space reconstruction velocity vector fields, and thus the process appear similar to a spatial treatment. In particular, the two vortices already shown are better reproduced. The same trend can be observed in streamlines plots which are smooth and absent of irregularities.

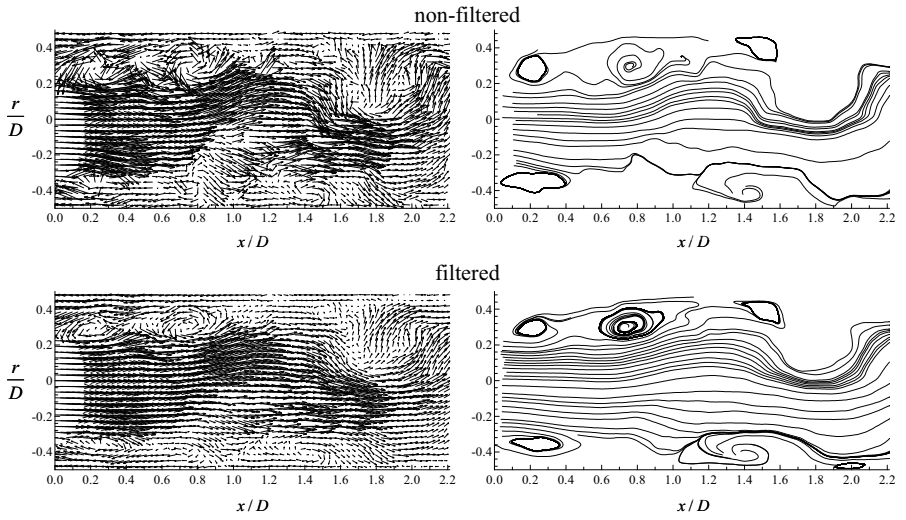

Fig. 4. Velocity vectors (left) and streamlines (right) for raw and filtered data at *Re* = 2000.

Another example of data post process is shown in Fig. 5. The velocity fluctuations obtained for *Re* = 560 is characterized by weak and low-frequency fluctuations so that instantaneous velocity map is highly subjected to noise. In contrast, use of the Wiener filter allows to remove main part of the noise and velocity map appears smooth. The same remark holds for vorticity map shown for *Re* = 640 where the differentiation process is highly sensitive to noise.

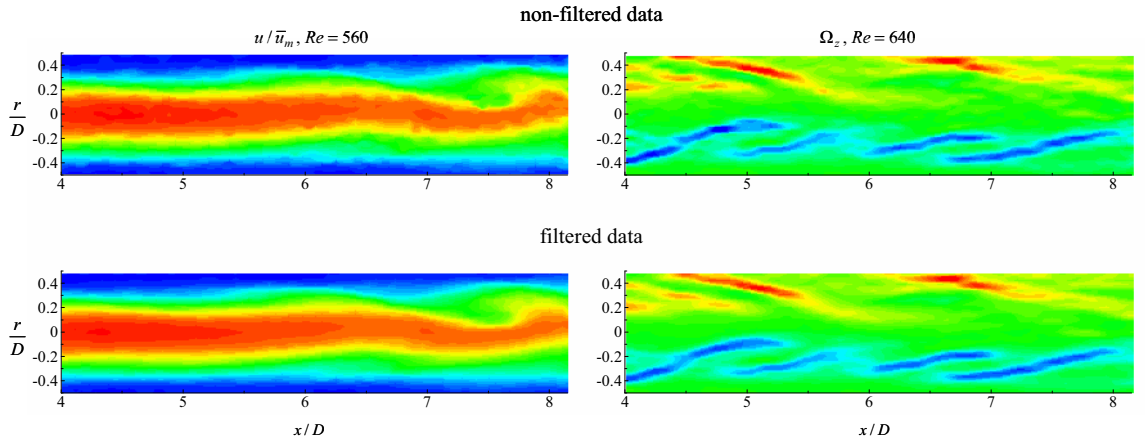

Fig. 5. Example of filtered results for a velocity map and a vorticity map.

3. Base Flow Characteristics

Mean velocity profiles downstream of the diffuser outlet are plotted in Fig. 6 for different Reynolds numbers. Close to the outlet ($x/D = 0$), mean velocity gradually decreases with increasing r from its maximum value obtained at centerline axis towards negative values before reaching the pipe wall where velocity is zero. A recirculation region is then observed and is the consequence of a flow separation occurring in the divergent part of the diffuser. For *Re* = 400, the velocity profile is almost self-similar whatever the axial position, pointing out that flow is not perturbed in this region. As *Re* increases, centerline velocity decreases with axial position; a transition in the shape of the velocity profile occurs and its location moves towards the diffuser outlet. For the highest *Re* value shown, profile becomes flat, velocity being almost constant in the pipe section except in boundary layer.

The shear-stress profiles are plotted in Fig. 7 for the same range as shown in Fig. 6. The

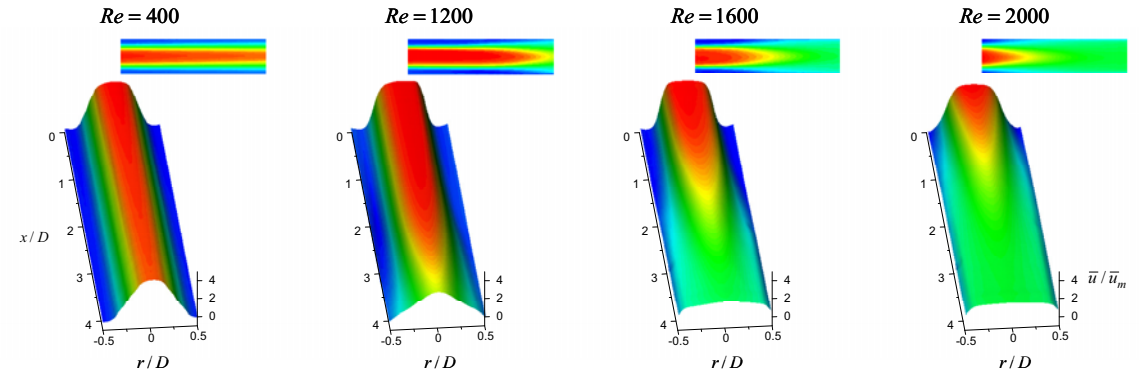

Fig. 6. Mean velocity profiles downstream of the diffuser.

absence of flow perturbations is confirmed for Re = 400 by shear-stress levels close to 0. For intermediate Reynolds numbers (Re = 1200 and Re = 1600), and for small axial positions, an axisymmetric shear-layer develops around the centerline region where the fluctuations are weak. Downstream, the shear-layer spreads transversally as the shear-stress value increases and reaches a maximum. The location of this maximum decreases with the Reynolds number, so that for Re = 2000, important fluctuations are observed directly at x/D = 0.

Fig. 7. Shear-stress profiles downstream of the diffuser.

From the above results, the general organization of the flow can be decomposed into three main regions, and can be illustrated with the Re = 1600 results. In the vicinity of the diffuser outlet the separated flow is similar to an axisymmetric free jet flow with presence of a potential core and development of an axisymmetric shear-layer (region 1, $0 < x/D < 2$). The potential core is not characterized by a spatially constant mean velocity but is defined by a region where fluctuation velocity levels are weak. Downstream, spatial amplification of the unstable layer induces flow perturbations towards the centerline and wall of the pipe, which defines the second region ($2 < x/D < 4$). This region is dominated by a jet-wall interaction where the jet can no longer be considered as a free jet due to confinement. Finally, far downstream, the flow gradually behaves like a pipe flow (region 3, $x/D > 4$). Additional results indicate that turbulence transition occurs between Re = 400 and Re = 800, a low value resulting from the introduction of an inflexion point into the velocity profile downstream of the diffuser contraction leading to transition. This result agrees with the value of Re = 722 obtained recently by Sherwin and Blackburn (2005) who analyzes the stability of a smooth 75 % stenosis flow with direct numerical simulations in order to examine the onset of turbulence.

4. Flow Unsteadiness

In view of the high level of velocity fluctuations observed, additional results were undertaken to characterize the unsteady and turbulent behavior of the flow by means of visual inspection. Figure 8 presents an example of the instantaneous character of the flow for several conditions. For Re = 520, evolution with time of axial velocity map shows the presence, for $x/D > 10$, of oscillations in the flow, characteristic of propagation of waves before formation and shedding of vortices. In the study

carried out by Bluestein et al. (1999) on vortex-shedding through a model of an arterial stenosis, periodic shedding began at approximately $Re = 375$.

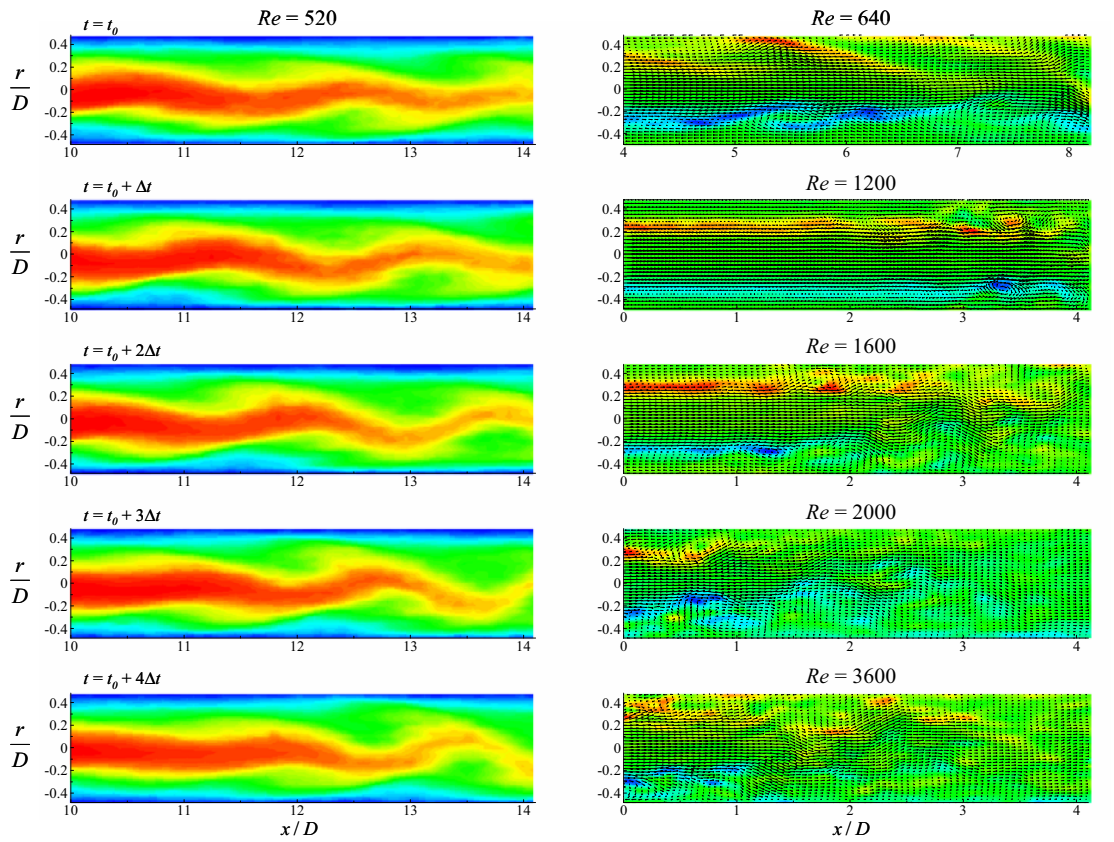

Fig. 8. Influence of the Reynolds number on the unsteady flow behavior.

At a Reynolds number of $Re = 640$, an instantaneous picture of the flow is better understood by the velocity vector field shown with the vorticity level of the component normal to the measurement plane. It is observed that the flow presents a superposition of elongated vorticity sheets which roll up to form conical structures. Positive and negative vorticity regions alternate and illustrate the development of a three-dimensional instability. For $Re = 1200$, and in the vicinity of the diffuser outlet, the vectors are parallel to the pipe axis and flow perturbations begin to occur for $x/D > 2$ in the upper part of the flow. The appearance of an instability after initial growth of the shear-layer is associated to a roll up and the shedding of a vortical structure is observed at $x/D \approx 3$. The process is the same for higher Reynolds numbers, but the vortex formation is localized at a distance which decreases from the outlet as Re increases. Moreover, the roll up is also accompanied downstream by a vortex breakdown leading to turbulence transition, like the flow pattern represented for $Re = 1600$. In the extreme case ($Re = 3600$), high fluctuating character of the flow show that the flow is already turbulent at the diffuser outlet.

5. Conclusion

An experimental set-up allowing time-resolved PIV velocity measurements has been built in order to characterize the flow in a smooth axisymmetric diffuser. The unsteady process and turbulence development have been analyzed with the influence of the Reynolds number. The use of an optimal filter, based on noise estimation in the frequency domain, showed an improvement of the quality of velocity vector fields and will be useful for further signal-processing.

In regards of the physic of the flow, the flow is computationally challenging for quantitative prediction when Reynolds number is close to the transition Reynolds number, which is the current case regarding natural blood flow conditions. In fact, a wide range of time and space scales is

encountered and therefore a numerical simulation requires lengthy integration times to obtain converged statistics as well as fine discretizations. It is also observed that the development of the shear-layer followed by roll-up of vortices and then vortex breakdown to turbulence can develop over a length of several diameters. This slow growth is a complex task for computation, but also for experimental models since the instability is very sensitive to upstream conditions and dissymmetry, even seemingly small. Moreover, for Reynolds numbers high enough to introduce an inflexion point into the velocity profile downstream of the diffuser contraction leading to transition, but small enough compared with the transition Reynolds number of pipe flows, a relaminarisation of the flow could occur far away from the outlet. These few remarks allow to point out the extreme complexity of the flow even if the geometry presents in appearance simple features.

References

Ahmed, S. A., An experimental investigation of pulsatile flow through a smooth constriction, Exptl. Thermal Fluid Sci., 17 (1998), 309-318.

Ahmed, S. A. and Giddens, D. P., Velocity measurements in steady flow through axisymmetric stenoses at moderate Reynolds numbers, J. Biomech., 16 (1983), 505-516.

Berger, S. A., Jou, L.-D., Flows in stenotic vessels, Annu. Rev. Fluid Mech., 32 (2000), 347-384.

Bluestein, D., Gutierrez, C., Mateo, L., Londono, M. and Schoephoerster, R. T., Vortex shedding in steady flow through a model of an arterial stenosis and its relevance to mural platelet deposition, Ann. Biomed. Eng., 27 (1999), 763-773.

Sherwin, S. J. and Blackburn, H. M., Three-dimensional instabilities and transition of steady and pulsatile axisymmetric stenotic flows, J. Fluid. Mech., 533 (2005), 297-327.

Simpson, R. L., Turbulent boundary-layer separation, Ann. Rev. Fluid Mech., 21 (1989), 205-234.

Son, S. Y. and Kihm, K. D., Evaluation of transient turbulent flow fields using digital cinematographic particle image velocimetry, Exp. in Fluids, 30 (2001), 537-550.

Author Profile

Jérôme Vétel: He received his Ph. D degree in 2001 from Poitiers University (ENSMA). He is a Post-Doctoral Fellow in the Mechanical Engineering Department of École Polytechnique Montréal. His current research interests include unsteady and turbulent flow, experimental techniques (PIV and hot wire anemometry) and signal processing.

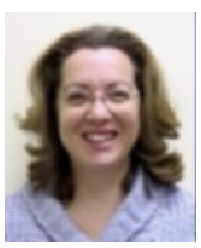

Marie-Isabelle Farinas: She received her Ph. D. degree in 2002 from École Polytechnique Montréal. She is currently a Research Scientist in the Mechanical Engineering Department of École Polytechnique Montréal. Her research interests include particle imaging velocimetry (PIV) technique, setup of experimental facilities for validation/verification, optimization and design methodology for small turbomachinery, FEM computational algorithms (mesh adaptation, free convection), control strategy for blood pumps (LVAD).

André Garon: He received his Ph. D. degree in 1987 from École Polytechnique Montréal. He is currently a Professor in Mechanical Engineering Department of École Polytechnique Montréal. His current research interests are focused on computational algorithm development and improvement, design and certification of a new left ventricular assist device (LVAD), setup of experimental facilities for validation/verification and he is also part of the ACE research team and CERCA hydraulic consortium.

Dominique Pelletier: He received his Ph. D. degree in 1984 from Virginia Polytechnic Institute & State University. He is currently a Professor in Mechanical Engineering Department of École Polytechnique Montréal. His research interests are sensitivity and uncertainty analysis of complex flows, adaptive remeshing for complex flows, error estimation for industrial FEM and CVFEM and analysis and design of industrial manufacturing process.